Time-dependent R -matrix theory for ultrafast atomic processes

Published in:
Physical Review A (Atomic, Molecular, and Optical Physics)

Document Version:
Publisher's PDF, also known as Version of record

Queen's University Belfast - Research Portal:
Link to publication record in Queen's University Belfast Research Portal

Time-dependent *R*-matrix theory for ultrafast atomic processes

M. A. Lysaght, H. W. van der Hart, and P. G. Burke

Centre for Theoretical Atomic, Molecular and Optical Physics, Queen's University Belfast, Belfast BT7 1NN, United Kingdom

We describe an *ab initio* nonperturbative time-dependent *R*-matrix theory for ultrafast atomic processes. This theory enables investigations of the interaction of few-femtosecond and -attosecond pulse lasers with complex multielectron atoms and atomic ions. A derivation and analysis of the basic equations are given, which propagate the atomic wave function in the presence of the laser field forward in time in the internal and external *R*-matrix regions. To verify the accuracy of the approach, we investigate two-photon ionization of Ne irradiated by an intense laser pulse and compare current results with those obtained using the *R*-matrix Floquet method and an alternative time-dependent method. We also verify the capability of the current approach by applying it to the study of two-dimensional momentum distributions of electrons ejected from Ne due to irradiation by a sequence of 2 as light pulses in the presence of a 780 nm laser field.

I. INTRODUCTION

The development of attosecond light sources [1,2] has enabled the observation of a wide variety of atomic processes on ultrashort time scales. Recent examples include the real-time observation of interference effects in double ionization of Ne using a combination of infrared and ultrashort pulses [3] and the stroboscopic study of single-ionization events in Ar [4]. Attosecond pulses have also opened up the possibility of studying inner-shell dynamics on ultrafast time scales [5] and have allowed for the profiling of the electric field of few-femtosecond laser pulses [6].

At present, the most advanced theoretical approaches for the description of atoms irradiated by intense short light fields are approaches dedicated to two-active-electron systems. The most sophisticated of these approaches is the so-called HELIUM approach of Parker and Taylor [7,8] in which the laser-driven two-electron problem is solved by a direct numerical integration of the full-dimensional time-dependent Schrödinger equation (TDSE). In this approach, the major challenge of accurately describing the correlation between the two electrons in He is treated without any significant approximations. The method has been particularly successful at describing recent measurements of electron distributions of singly and doubly ionized He in an intense 390 nm laser field [9].

Although the full-dimensional approach has enjoyed much success at describing single and double ionizations of He in strong laser fields, its application to treating complex atoms with more than two electrons is currently computationally intractable. The problem of accurately describing multielectron atoms, such as Ne and Ar, in intense short laser pulses therefore requires the development of other computationally tractable methods. One such method is the *R*-matrix Floquet (RMF) approach [10] which combines the traditional time-independent *R*-matrix method [11] with a Floquet expansion of the driven time-dependent wave function. In the *R*-matrix method configuration space is separated into two regions: an inner region in which all interactions between the electrons and the laser field are described in full detail and an outer region in which only long-range interactions are in-

cluded. Over the last two decades the RMF approach has been successfully employed to describe a wide range of atomic multiphoton processes [12–15]. This is an *ab initio* theory, which is fully nonperturbative and is applicable to arbitrary multielectron atoms and atomic ions, allowing an accurate description of electron-electron correlation effects. However, because this theory is based on the Floquet-Fourier ansatz, its applications are confined to treating laser pulses involving many cycles of the field, typically exceeding several tens of femtoseconds in length. For the description of complex atoms in ultrashort light fields, however, a direct integration of the TDSE is required.

So far, the most advanced time-dependent numerical simulations for complex multielectron atoms, such as Ne and Ar, irradiated by ultrashort light fields have employed the single-active-electron (SAE) approximation [16], in which the electrons are assumed to be effectively independent and only the electron that is emitted is assumed to be "active." However, recent experiments have shown that the response of multielectron atoms to ultrashort pulses consists of a coherent response of many electrons [3]. For example, due to the high-frequency components of the ultrashort pulse, shake-up states can be populated resulting in Auger transitions that occur on a femtosecond time scale. Since the light pulse duration is on the order of attoseconds, approaches are required that can reliably describe such ultrafast multielectron rearrangement dynamics.

We therefore recently initiated the development of time-dependent *R*-matrix (TDRM) theory to describe complex multielectron atoms in intense ultrashort light pulses. TDRM theory was first proposed by Burke and Burke [17] for the solution of a one-dimensional model problem. The goal of our recent efforts has been to extend the one-dimensional method to a three-dimensional (3D) method for the realistic and accurate treatment of complex multielectron atoms in intense ultrashort light fields. As an initial approach we introduced an *ab initio* time-dependent method that employs *R*-matrix basis functions in a box to investigate multiphoton ionization of complex atoms [18]. The method, in which the calculations are performed within an *R*-matrix inner (RMI) region only, has been shown to give accurate results for multiphoton ionization of Ar irradiated by a 390 nm laser pulse

[18]. We recently extended the RMI method by significantly increasing the size of the box in which the calculations are performed and also the number of continuum functions used to describe the outgoing electron. By doing so we have been able to study wave-packet interference effects on the two-dimensional (2D) momentum distributions of electrons ejected from Ne irradiated by a sequence of 2 as pulses in the presence of a 390 nm laser field [19]. We note that an alternative RMI method has been developed independently from us, which has been used to study multiphoton ionization of Ne and Ar [20,21].

Although the RMI method has been successful at describing multielectron atoms in ultrashort laser fields, it is not a truly time-dependent R-matrix theory, in that it does not exploit the natural division of configuration space occurring in R-matrix theory, i.e., the reduction of the laser-atom problem into a "complex" inner region close to the nucleus, in which electron-electron interactions are fully described, and a "simple" outer region in which an effective one-electron problem is solved. As a result, any increase in the size of the spatial region in which the calculations are performed will place severe demands on computational resources.

In the most recent stage of our efforts, we have completed the development of a full 3D TDRM method that includes the R-matrix outer region. The method has recently been applied to describe a proposed attosecond pump-probe experiment that combines the use of a free-electron laser (FEL) pulse and an attosecond pulse to explore ultrafast excitation dynamics in Ne [22]. In this paper we describe the full 3D TDRM theory in greater detail. The method can be used to accurately describe the interaction of intense ultrashort light fields with arbitrary multielectron atoms and atomic ions. As a means of demonstrating the accuracy of the TDRM method we first apply it to the study of electron wave packets ejected from Ne irradiated by a FEL pulse and compare results using the current method with those obtained using the RMI and RMF methods. We also reveal the capability of the method by applying it to the study of electron wave packets ejected from Ne irradiated by a sequence of two ultrashort pulses in the presence of a 780 nm laser field.

II. TIME-DEPENDENT R-MATRIX THEORY

A. Basic theory

In this section we describe an *ab initio* time-dependent R-matrix theory of multiphoton ionization of atoms or atomic ions by an intense ultrashort laser pulse, where we assume that the atom or ion contains $N+1$ electrons and has a nuclear charge Z. We also assume that the laser field, which is treated classically using the dipole approximation, is linearly polarized, spatially homogeneous, and is described by the vector potential $\mathbf{A}(t)$. Neglecting relativistic effects, the atomic system in the presence of the laser field is then described by the TDSE which we write here as

$$H(t)\Psi(\mathbf{X}_{N+1},t) = i\frac{\partial}{\partial t}\Psi(\mathbf{X}_{N+1},t), \qquad (1)$$

where

$$H(t) = H_{N+1} + \frac{1}{c}\mathbf{A}(t)\cdot\mathbf{P}_{N+1} + \frac{N+1}{2c^2}\mathbf{A}^2(t). \qquad (2)$$

In this equation $\mathbf{P}_{N+1}=\Sigma_{i=1}^{N+1}\mathbf{p}_i$ is the total electron momentum operator and H_{N+1} is the nonrelativistic Hamiltonian of the $(N+1)$-electron atom or ion in the absence of the laser field defined by

$$H_{N+1} = \sum_{i=1}^{N+1}\left(-\frac{1}{2}\nabla_i^2 - \frac{Z}{r_i} + \sum_{i>j=1}^{N+1}\frac{1}{r_{ij}}\right), \qquad (3)$$

where we have taken the origin of the coordinates to be in the target nucleus, which we assume to have infinite mass, and we have written $r_{ij}=|\mathbf{r}_i-\mathbf{r}_j|$ where $\mathbf{r}_i$ and $\mathbf{r}_j$ are the vector coordinates of the ith and jth electrons. Also in Eq. (1), $\mathbf{X}_{N+1}\equiv\mathbf{x}_1,\mathbf{x}_2,\dots,\mathbf{x}_{N+1}$, where $\mathbf{x}_i\equiv\mathbf{r}_i\sigma_i$ are the space and spin coordinates of the electron.

As discussed in the previous section, the RMF approach for solving Eq. (1) is not applicable for ultrashort light fields and we must therefore solve this equation directly using time-dependent theory. In the rest of this paper we consider the solution of Eq. (1) using the dipole length gauge in both the R-matrix internal and external regions. This use of the length gauge is in contrast to strong-field calculations for one-electron and two-electron systems in which the velocity form of the dipole operator is preferred. However, based on previous investigations, using the RMI method [18], we have found that, for the interaction of the laser field with a multielectron atom, the laser field is best described using the length form of the dipole operator. The velocity gauge appears to be less appropriate for multielectron systems since it emphasizes short-range multielectron excitations near the nucleus. As a consequence, the velocity gauge description of the laser field requires a far better description of the atomic structure than the length form of the dipole operator, placing a greater computational demand on calculations using this gauge. It should also be noted that in RMF theory the length gauge is also used in the internal region but a transformation is made to the velocity gauge in the external region and possibly to the acceleration frame in the asymptotic region. This is because in RMF theory the external and asymptotic regions extend out to infinity where the length gauge diverges. This does not happen in TDRM theory when the time frame does not exceed a few tens of femtoseconds. Also, the transformation from the length gauge to the velocity gauge on the R-matrix boundary $r=a_0$ would have to be carried out at each time step in TDRM theory which would introduce accumulated errors.

In order to solve the TDSE in the dipole length gauge we transform Eq. (1) using the unitary gauge transformation

$$\Psi(\mathbf{X}_{N+1},t) = \exp\left[-\frac{i}{c}\mathbf{A}(t)\cdot\mathbf{R}_{N+1}\right]\Psi^L(\mathbf{X}_{N+1},t), \qquad (4)$$

which yields the following time-dependent equation:

$$[H_{N+1} + \mathbf{E}(t)\cdot\mathbf{R}_{N+1}]\Psi^\mathbf{L}(\mathbf{X}_{N+1},t) = i\frac{\partial}{\partial t}\Psi^\mathbf{L}(\mathbf{X}_{N+1},t), \quad (5)$$

where $\mathbf{E}(t)$ is the electric field of the laser pulse and $R_{N+1}=\Sigma_{i=1}^{N+1}\mathbf{r}_i$. The boldface superscript **L** indicates that the inter-

acting electrons are described in the dipole length gauge and will be dropped for the rest of the paper.

We now write Eq. (5) in the form

$$i\frac{\partial}{\partial t}\Psi(\mathbf{X}_{N+1},t) = [H_{N+1} + H_{\text{int}}(t)]\Psi(\mathbf{X}_{N+1},t), \qquad (6)$$

where

$$H_{\text{int}}(t) = \mathbf{E}(t) \cdot \sum_{i=1}^{N+1} \mathbf{r}_i \qquad (7)$$

in the dipole length gauge. We then introduce a discrete mesh in time defined by

$$t_q = q\Delta t, \quad q = 0,1,2\ldots, \qquad (8)$$

where Δt is the time interval. The solution of Eq. (6) at $t=t_{q+1}$ can then be expressed in terms of the solution at $t=t_q$ as follows:

$$\Psi(\mathbf{X}_{N+1},t_{q+1}) = \frac{1 - \frac{1}{2}i\Delta t H(t_{q+1/2})}{1 + \frac{1}{2}i\Delta t H(t_{q+1/2})}\Psi(\mathbf{X}_{N+1},t_q) + O(\Delta t^3),$$

$$(9)$$

where we have used the unitary Cayley form of the time evolution operator $\exp[-itH(t)]$ and here we have written

$$t_{q+1/2} = t_q + \frac{1}{2}\Delta t. \qquad (10)$$

If we neglect terms of $O(\Delta t^3)$ then Eq. (9) can be rewritten as

$$[H(t_{q+1/2}) - E]\Psi(\mathbf{X}_{N+1},t_{q+1}) = \Theta(\mathbf{X}_{N+1},t_q), \qquad (11)$$

where

$$\Theta(\mathbf{X}_{N+1},t_q) = -[H(t_{q+1/2}) + E]\Psi(\mathbf{X}_{N+1},t_q), \qquad (12)$$

and where $H(t_{q+1/2})$ is the time-dependent Hamiltonian at the midpoint. In this formalism the imaginary energy defines the time step as $E \equiv 2i\Delta t^{-1}$. Equation (11) is an inhomogeneous equation where the right-hand side can be calculated if the wave function at time $t=t_q$ is known. Solving this equation then yields the wave function at time $t=t_{q+1}$. Hence this equation enables the solution to be propagated forward in time.

In the rest of this paper we present a theoretical analysis of our *R*-matrix method for solving Eq. (11) which enables the wave function to be propagated forward in time through one time step from $t=t_q$ to $t=t_{q+1}$. The solution of this equation is accomplished by partitioning configuration space into two regions as shown in Fig. 1. We note that unlike the partitioning scheme in *R*-matrix Floquet theory, described by Burke *et al.* [10], we omit the asymptotic region since we make the external region large enough, so that the ejected-electron wave function vanishes by the outer boundary $r=a_p$. However, the conditions used to define the boundary $r=a_0$ between the internal and external regions are the same as in the *R*-matrix Floquet theory. That is, in the inner region electron exchange and electron-electron correlation effects between the ejected electron and the remaining *N* electrons are important, while in the outer region electron exchange
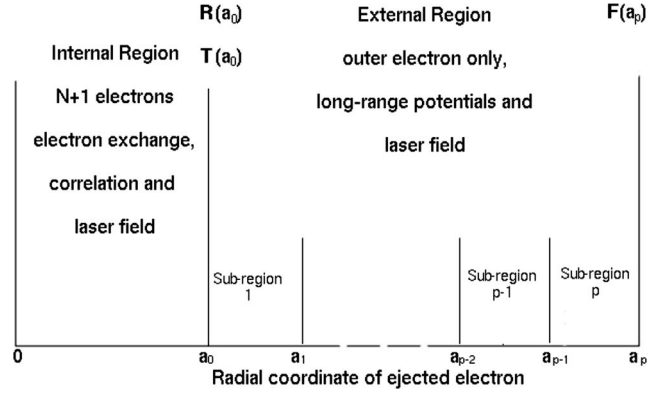

FIG. 1. Partitioning of configuration space in time-dependent *R*-matrix theory.

and correlation effects between the ejected electron and the remaining *N* electrons are negligible, and hence the ejected electron moves in the local long-range multipole potential of the residual *N*-electron atom or atomic ion together with the laser field.

B. Internal region analysis

In order to solve Eq. (11) in the internal region we expand the wave function $\Psi(\mathbf{X}_{N+1},t_{m+1})$ in Eq. (11) in a completely antisymmetric *R*-matrix basis $\psi_k(\mathbf{X}_{N+1})$ as follows:

$$\Psi_j^\gamma(\mathbf{X}_{N+1},t_{m+1}) = \sum_k \psi_k^\gamma(\mathbf{X}_{N+1})A_{kj}^\gamma(t_{m+1}). \qquad (13)$$

In this equation, j labels the solution of Eq. (11) which corresponds to the initial bound state of the atom or ion before the laser is switched on and $A_{kj}^\gamma(t_{m+1})$ are the time-dependent expansion coefficients, which depend on the boundary conditions satisfied by the wave function Ψ_j^γ at the initial time $t=0$. Also, we have introduced the superscript γ representing the quantum numbers which depend on the symmetry of the atomic state and the polarization of the laser photons. For the nonrelativistic case described here γ is given by

$$\gamma = \alpha S M_S M_L \pi', \qquad (14)$$

where S is the total spin angular-momentum quantum number, M_S and M_L are the total spin and orbital magnetic quantum numbers, π' is the product of the parities of the photons and the target state, and α serves to specify the remaining quantum numbers.

We now expand the basis functions ψ_k^γ in Eq. (13) in a close coupling with pseudostates expansion given by

$$\psi_k(\mathbf{X}_{N+1}) = \mathcal{A}\sum_{pl} \bar{\Phi}_p^\gamma(\mathbf{X}_N; \hat{r}_{N+1}\sigma_{N+1})r_{N+1}^{-1}u_{pl}(r_{N+1})a_{plk}$$

$$+ \sum_p \eta_p^\gamma(\mathbf{X}_{N+1})b_{pk}. \qquad (15)$$

In this equation $\mathcal{A}$ is the usual antisymmetrization operator and $\bar{\Phi}_p^\gamma$ are time-independent channel functions which are formed by coupling the residual atom or ion state Φ_i, with the angular and spin functions $Y_{l_i m_{l_i}}$ and $\chi_{(1/2)m_i}$ of the ejected

electron. The residual atom or ion states Φ_i are chosen to diagonalize the residual ion Hamiltonian H_N as follows:

$$\langle \Phi_i | H_N | \Phi_j \rangle = E_i \delta_{ij}, \tag{16}$$

where H_N is defined by Eq. (3) with $N+1$ replaced with N. Also in Eq. (15) u_{pl} are the time-independent radial basis functions which are nonvanishing on the boundary of the internal region and η_p^γ are time-independent quadratically integrable antisymmetric functions, which are included to represent electron-electron correlation effects which vanish at the boundary of the internal region. a_{plk} and b_{pk} are time-independent coefficients obtained from a field-free diagonalization. The summation variable p in the first expansion in Eq. (15) represents both quantum numbers L and i. We assume in Eq. (15), and later equations, that n channel functions $\bar{\Phi}_p^\gamma$ are retained so that the index p goes over 1 to n. Also, we assume that, in the first expansion, n_c radial basis functions u_{pl}, $l=1,\ldots,n_c$ are included in each channel. Finally, in the second expansion in Eq. (15), the summation variable p goes over n_b quadratically integrable functions, η_p^γ, which vanish at the boundary of the internal region. These functions are included to allow for other short-range correlation effects in the internal region that are not adequately represented by the first expansion in Eq. (15). It should also be noted that pseudostates are retained in Eq. (15) to represent high-lying continuum states of the residual ion. We find it convenient to rewrite Eq. (15) in the concise form

$$\psi_k(\mathbf{X}_{N+1}) = \sum_{k'=1}^{n_t} \xi_{k'}(\mathbf{X}_{N+1}) c_{k'k}, \tag{17}$$

where $k=1,\ldots,n_t$ and $n_t=nn_c+n_b$ is the total number of linearly independent basis functions $\xi_k(\mathbf{X}_{N+1})$ retained in the expansion in Eq. (15) and $c_{k'k}$ represents the coefficients a_{plk} and b_{pk}.

In order to solve equation Eq. (11) in the inner region to yield the wave function $\Psi(\mathbf{X}_{N+1}, t_{q+1})$, we observe that the Hamiltonian $H(t_{q+1/2})$ is not Hermitian in this region owing to the presence of the kinetic energy $-\frac{1}{2}\nabla_i^2$ term in $H(t_{q+1/2})$. Consequently we introduce the Bloch operator

$$\mathcal{L} = \frac{1}{2} \sum_{i=1}^{N+1} \delta(r_i - a_0) \left(\frac{d}{dr_i} - \frac{b_0 - 1}{r_i} \right), \tag{18}$$

such that $H_{N+1} + \mathcal{L}$ is Hermitian in the internal region for any value of the arbitrary constant b_0.

Using this result we can rewrite Eq. (11) in the internal region as

$$(H + \mathcal{L} - E)\Psi = \mathcal{L}\Psi + \Theta, \tag{19}$$

which has the formal solution

$$\Psi = (H + \mathcal{L} - E)^{-1}(\mathcal{L}\Psi + \Theta), \tag{20}$$

where for notational simplicity we have omitted the arguments in H, Ψ, and Θ. Equation (11) then becomes

$$|\Psi\rangle = \sum_{k,k'} |\psi_k\rangle\langle\psi_k| \frac{1}{H + \mathcal{L} - E} |\psi'_k\rangle\langle\psi'_k| [\mathcal{L}|\Psi\rangle + |\Theta\rangle], \tag{21}$$

which can be written as

$$\Psi(\mathbf{X}_{N+1}, t_{q+1}) = \sum_k \psi_k(\mathbf{X}_{N+1}) B_k(E, t_{q+1}), \tag{22}$$

where the summation is over the total number of linearly independent basis functions retained in the expansion in Eq. (15). Our objective is to determine the coefficients $B_k(E, t_{q+1})$ which express the wave function $\Psi(\mathbf{X}_{N+1}, t_{q+1})$ in the internal region in terms of the R-matrix basis functions $\psi_k(\mathbf{X}_{N+1})$ defined by Eq. (15).

In order to achieve this objective we project Eq. (21) onto the n channel functions $\bar{\Phi}_p^\gamma$ and evaluate it on the boundary $r_{N+1} = a_0$ of the internal region. We obtain

$$F_p(a_0) = \sum_{p'=1}^n R_{pp'}(E) a_0 \bar{F}_{p'}(a_0) + T_p(a_0), \tag{23}$$

where $p=1,\ldots,n$ and where the reduced radial-wave functions $F_p(a_0)$ are defined by

$$F_p(a_0) = \langle \bar{\Phi}_p^\gamma(\mathbf{X}_N; \hat{\mathbf{r}}_{N+1}\sigma_{N+1}) r_{N+1}^{-1} | \Psi \rangle'_{r_{N+1}=a_0}, \tag{24}$$

where $p=1,\ldots,n$ and where we note that the prime on the matrix elements in this and later equations means that the integral is carried out over space and spin coordinates of all $N+1$ electrons except the radial coordinate r_{N+1} of the ejected electron. The R-matrix elements $R_{pp'}(E)$ in Eq. (23) are defined by

$$R_{pp'}(E) = \frac{1}{2a_0} \sum_{kk'} \omega_{pk} \left(\frac{1}{H + \mathcal{L} - E} \right)_{kk'} \omega_{p'k'}, \tag{25}$$

where $p, p' = 1,\ldots,n$ and where the surface amplitudes ω_{pk} are defined by

$$\omega_{pk} = \langle \bar{\Phi}_p^\gamma(\mathbf{X}_N; \hat{\mathbf{r}}_{N+1}\sigma_{N+1}) r_{N+1}^{-1} | \psi_k \rangle'_{r_{N+1}=a_0}, \tag{26}$$

where $p=1,\ldots,n$; $k=1,\ldots,n_t$. Also, the modified derivative functions $\bar{F}_p(a_0)$ in Eq. (23) are defined by

$$\bar{F}_p(a_0) = \left. \frac{dF_p}{dr} \right|_{r=a_0}, \quad p=1,\ldots,n. \tag{27}$$

Finally, the inhomogeneous vector $T_p(a_0)$ in Eq. (23) is defined by

$$T_p(a_0) = \sum_{kk'} \omega_{pk} \left(\frac{1}{H + \mathcal{L} - E} \right)_{kk'} S_k, \quad p=1,\ldots,n, \tag{28}$$

where it follows from Eqs. (11) and (12) that

$$S_k = \langle \psi_k | \Theta \rangle, \quad k=1,\ldots,n_t. \tag{29}$$

The wave function $\Psi(\mathbf{X}_{N+1}, t_q)$ in Eq. (29) has been obtained at the end of the previous time step $t=t_q$ and is thus known. Hence the vector S_k and all the quantities on the right-hand side of Eq. (29) can be calculated and the inhomogeneous vector $T_p(a_0)$ can be determined.

Returning to Eqs. (21) and (22), the coefficients $B_k(E, t_{q+1})$ can now be written as

$$B_k(E, t_{q+1}) = \left(\frac{1}{H + \mathcal{L} - E} \right)_{kk'} \left(\frac{1}{2} \sum_{p=1}^{n} \omega_{pk} \bar{F}_p(a_0) + S_k \right),$$
(30)

where $k = 1, \ldots, n_t$ and where ω_{pk}, $\bar{F}_p(a_0)$, and S_k are defined by Eqs. (26), (27), and (29) respectively. The only unknown in this definition of $B_k(E, t_{q+1})$ is $\bar{F}_p(a_0)$ which we will see in the rest of this paper can be determined from the results of the propagation in the external region. Hence $B_k(E, t_{q+1})$ can be calculated and the wave function $\Psi(\mathbf{X}_{N+1}, t_{q+1})$, which provides the starting point for the calculation in the next time step, can be determined from Eq. (22). It should be noted at this point that in our current computational implementation of the TDRM method, we apply a linear solver approach to Eq. (21) at each time step, in order to obtain the *R* matrix and *T* vector at the inner region boundary. Alternatively, the *R* matrix and *T* vector can be obtained by diagonalizing the operator $H + \mathcal{L} - E$ in the *R*-matrix basis described by Eq. (15) at each time step. This diagonalization of the operator $H + \mathcal{L} - E$ at each time step could be made more efficient using an iterative procedure [23] where in this method the result from the previous time step would be used as a starting point. A similar iterative procedure could also be used to solve the simultaneous equations at each time step, which could prove useful for very large matrices.

In concluding this internal region analysis, it is convenient for future reference to rewrite Eq. (23) in matrix notation as

$$\mathbf{F}(a_0) = \mathbf{R}a_0\bar{\mathbf{F}}(a_0) + \mathbf{T}(a_0),$$
(31)

where

$$\bar{\mathbf{F}}(a_0) = \left(\frac{d\mathbf{F}}{dr} \right)_{r=a_0}.$$
(32)

The *R* matrix **R** and the inhomogeneous vector **T** at $r = a_0$ are defined by Eqs. (25) and (28), respectively. These quantities then provide the boundary condition for propagating **R** and **T** in the external region as described below.

C. External region analysis

We now consider the solution of Eq. (11) in the external region. In this region we expand the wave function as follows:

$$\Psi(\mathbf{X}_{N+1}, t_{q+1}) = \sum_{p=1}^{n} \bar{\Phi}_p^\gamma(\mathbf{X}_N; \hat{\mathbf{r}}_{N+1}\sigma_{N+1}) r_{N+1}^{-1} F_p(r_{N+1}),$$
(33)

where $a_0 \leq r_{N+1} \leq a_p$ and where, as in the internal region, we have omitted the time dependence in $F_p(r_{N+1})$. As in Eq. (15), the subscript *p* represents the channel quantum numbers *L* and *i*. The reduced radial functions $F_p(r)$ in Eq. (33) are analytical continuations of the functions which are defined by Eq. (24) on the boundary of the internal region.

Coupled second order differential equations satisfied by the reduced radial-wave functions $F_p(r)$, which represent the motion of the electron in the *p*th channel, can be obtained by substituting Eq. (33) into Eq. (11) and projecting onto the channel functions $\bar{\Phi}_p^\gamma$. In order to solve the coupled inhomogeneous second-order differential equations, we first write them in standard matrix form as follows:

$$(\mathbf{H} - E\mathbf{I})\mathbf{F}(r) = \boldsymbol{\theta}(r),$$
(34)

where the Hamiltonian matrix **H** is now defined by

$$\mathbf{H} = -\frac{1}{2} \left(\mathbf{I}\frac{d^2}{dr^2} + \mathbf{V}(r) - 2\mathbf{W}(r) + \mathbf{k}^2 \right),$$
(35)

where **I** is the unit matrix and $\mathbf{V}(r)$ is given by

$$\mathbf{V}(r) = -\frac{l(l+1)}{r^2} + \frac{2(Z-N)}{r}$$
(36)

and $\mathbf{k}^2$ can be expressed in terms of the diagonal energy eigenvalue matrix **E** of the residual *N*-electron atom or ion by the equation

$$\mathbf{k}^2 = -2\mathbf{E}.$$
(37)

Also in Eq. (35), $\mathbf{W}(r)$ is the long-range potential matrix coupling the channels which is given by

$$\mathbf{W} = \mathbf{W}_E + \mathbf{W}_D + \mathbf{W}_P.$$
(38)

Here $\mathbf{W}_E$ arises from the electron-electron and electron-nuclear potential terms in the Hamiltonian $H(t_{q+1/2})$, while $\mathbf{W}_D$ and $\mathbf{W}_P$ arise, respectively, from the interaction of the light field with the residual *N*-electron atom or ion and from the interaction of the light field with the ejected electron. Explicit expressions for the potential matrices $\mathbf{W}_E$, $\mathbf{W}_D$, and $\mathbf{W}_P$ can be found in the Appendix. It should be noted that here we use the length gauge in the external region rather than the velocity gauge as is the case in [10]. Finally, the inhomogeneous term $\boldsymbol{\theta}(r)$ in Eq. (34) is defined for a single channel by

$$\theta_p(r) = \langle \bar{\Phi}_p^\gamma(\mathbf{X}_N; \hat{\mathbf{r}}_{N+1}\sigma_{N+1}) r_{N+1}^{-1} | \Theta \rangle,$$
(39)

where Θ has already been defined in Eq. (12) and where we have omitted the time variable in $\theta(r)$ and in the potential terms $\mathbf{W}(r)$ in Eq. (35) for notational convenience. The complex energy *E* in Eqs. (34) and (37) can be conveniently measured from the lowest threshold of the residual atom or ion.

In order to solve Eq. (34), we now introduce the Bloch operator $\mathcal{L}_s$ defined by the equation

$$\mathcal{L}_s = \frac{1}{2}\mathbf{I} \left(\delta(r - a_s)\frac{d}{dr} - \delta(r - a_{s-1})\frac{d}{dr} \right),$$
(40)

such that $\mathbf{H} + \mathcal{L}_s$ is Hermitian over the subregion $a_{s-1} \leq r \leq a_s$ in the space of functions satisfying arbitrary boundary conditions at $r = a_{s-1}$ and $r = a_s$. We can then rewrite Eq. (34) in the *s*th subregion as

$$(\mathbf{H} + \mathcal{L}_s - E\mathbf{I})\mathbf{F}(r) = \mathcal{L}_s\mathbf{F}(r) + \boldsymbol{\theta}(r),$$
(41)

which has the formal solution

$$\mathbf{F}(r) = (\mathbf{H} + \boldsymbol{\mathcal{L}}_s - E\mathbf{I})^{-1}[\boldsymbol{\mathcal{L}}_s\mathbf{F}(r) + \boldsymbol{\theta}(r)]. \qquad (42)$$

The Green's function in this equation is defined as the solution of the following equation in the subregion:

$$(\mathbf{H} + \boldsymbol{\mathcal{L}}_s - E\mathbf{I})\mathbf{G}_s(r,r') = \frac{1}{2}\mathbf{I}\delta(r-r'). \qquad (43)$$

We use a similar method introduced by Baluja *et al.* [24] to obtain a spectral representation of $\mathbf{G}_s(r,r')$ in Eq. (43) where, in this case, instead of using a basis of orthonormal shifted Legendre polynomials, we use a basis of B splines and solve a system of linear equations in each subregion. It should be noted that implementing the approach by using B splines as a basis set adds complexity to the evaluation of the linear equations in the external region due to their nonorthogonality, and that the analysis given here is with respect to the use of orthonormal functions as a basis set.

We can now rewrite Eq. (43) with $a_{s-1} \le r \le a_s$ as

$$\mathbf{F}(r) = 2\int_{a_{s-1}}^{a_s} \mathbf{G}_s(r,r')\boldsymbol{\mathcal{L}}_s\mathbf{F}(r')dr' + \mathbf{J}(r), \qquad (44)$$

where

$$\mathbf{J}(r) = 2\int_{a_{s-1}}^{a_s} \mathbf{G}_s(r,r')\boldsymbol{\theta}(r')dr'. \qquad (45)$$

Evaluating Eq. (44) at $r=a_{s-1}$ and $r=a_s$ then yields the following equations:

$$\mathbf{F}(a_{s-1}) = \mathbf{R}_{s-1}a_{s-1}\left(\frac{d\mathbf{F}}{dr}\right)_{r=a_{s-1}} + \mathbf{T}(a_{s-1}) \qquad (46)$$

and

$$\mathbf{F}(a_s) = \mathbf{R}_s a_s\left(\frac{d\mathbf{F}}{dr}\right)_{r=a_s} + \mathbf{T}(a_s), \qquad (47)$$

where in this case the R matrix and T vector on the boundary $r=a_0$ of the internal region are given by Eqs. (25) and (28). We then obtain the following outward propagation equations for $\mathbf{R}_s$ and $\mathbf{T}(a_s)$:

$$a_s\mathbf{R}_s = \mathbf{G}_s(a_s,a_s) - \mathbf{G}(a_s,a_{s-1})[\mathbf{G}_s(a_{s-1},a_{s-1}) + a_{s-1}\mathbf{R}_{s-1}]^{-1}$$
$$\times \mathbf{G}_s(a_{s-1},a_s), \qquad (48)$$

$$\mathbf{T}(a_s) = \mathbf{J}(a_s) + \mathbf{G}_s(a_s,a_{s-1})[\mathbf{G}_s(a_{s-1},a_{s-1}) + a_{s-1}\mathbf{R}_{s-1}]^{-1}$$
$$\times [\mathbf{T}(a_{s-1}) - \mathbf{J}(a_{s-1})]. \qquad (49)$$

Finally we obtain the following inward propagation equation for the wave function:

$$\mathbf{F}(a_{s-1}) = a_{s-1}\mathbf{R}_{s-1}[\mathbf{G}_s(a_{s-1},a_{s-1}) + a_{s-1}\mathbf{R}_{s-1}]^{-1}$$
$$\times \{\mathbf{G}_s(a_{s-1},a_s)a_s^{-1}\mathbf{R}_s^{-1}[\mathbf{F}(a_s) - \mathbf{T}(a_s)]$$
$$+ \mathbf{G}_s(a_{s-1},a_{s-1})a_{s-1}^{-1}\mathbf{R}_{s-1}^{-1}\mathbf{T}(a_{s-1}) + \mathbf{J}(a_{s-1})\}. \qquad (50)$$

The wave function for all values of r can then be obtained from Eq. (44) and hence the inhomogeneous terms in Eqs. (11) and (34) can be calculated for the next time integration step. In this way Eq. (11) can be stepped forward in time for all positive t_q given the wave function at time $t=0$. The results for multiphoton ionization of Ne discussed below indicate that this procedure is stable.

III. APPLICATION TO NEON

As a first step to verifying the accuracy of the present TDRM method we investigate electron wave packets ejected from Ne irradiated by a laser pulse with a central photon energy $\omega_0 = 17$ eV and compare results obtained using the current method with results obtained using the RMI method. The RMI method has recently been developed by both the present authors [18] and by a separate group [20] and has been established as a highly accurate method for obtaining multiphoton ionization rates for multielectron atoms.

For both the RMI and TDRM calculations in the R-matrix inner region we use the R-matrix basis developed for single-photon ionization of Ne [25]. In the case of the TDRM calculations, we use an inner region radius of 20 a.u. The set of continuum orbitals contains 60 continuum functions for each available angular momentum l of the continuum electron. The results presented here have been obtained including only the $1s^2 2s^2 2p^5 \, ^2P^o$ ground state of Ne$^+$ as a target state. Details on all the orbital functions used in the calculation can be found in Ref. [25]. The description of Ne includes all $1s^2 2s^2 2p^5 \varepsilon l$ channels up to $L=L_{max}$ where $L_{max}=5$. In the outer region we propagated the R matrix and T vector outward to a radial distance of 200 a.u. in order to prevent any reflections of the wave function from the outer region boundary. Each external region sector was typically 3 a.u. wide and contained 35 B splines per channel with order $k=9$. For the RMI calculations, we used a box size of 140 a.u. with 100 continuum functions for each available angular momentum l of the continuum electron. Similar pulse shapes to those used in Ref. [18] have been used here with a three-cycle sin^2 turn on of the electric field followed by a three-cycle sin^2 turn off. In the calculations we used a laser pulse with a peak intensity $I_0 = 5 \times 10^{13}$ W/cm^2 and we typically use 200 time steps per cycle.

Figure 2 shows the real part of the ^1S ($l=1$) partial continuum wave function of Ne calculated 1.46 fs (6 cyles) after the end of the 6 cycle 17 eV laser field. The blue solid thin line shows the R-matrix outer region part of the wave function obtained using the present TDRM method and the black dashed-dotted line shows the corresponding R-matrix inner region part of the wave function. The TDRM results are compared to results obtained using the RMI method (red dashed line). The comparison of the time-dependent wave functions obtained using the current TDRM method to those obtained using the highly accurate RMI method represents one of the most stringent tests of accuracy for the present TDRM method. The excellent agreement between the results of the two independent methods as is evident in Fig. 2 verifies the accuracy and reliability of the TDRM method. We have also compared the results for the other ionization channels included in the calculation and have found the same level of agreement between the two methods.

As a second means of demonstrating the accuracy of the current TDRM method, we compare two-photon ionization
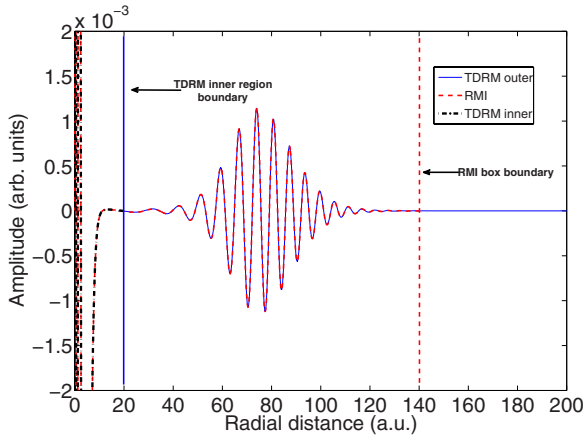
FIG. 2. (Color online) Real part of the ^1S ($l=1$) partial continuum wave function of Ne calculated 1.46 fs (6 cycles) after the end of the 6 cycle 17 eV laser field. The blue solid line shows the *R*-matrix outer region part of the wave function obtained using the present TDRM method and the black dashed-dotted line shows the corresponding *R*-matrix inner region part of the wave function. The TDRM results are compared to results obtained using the RMI method (red dashed line).
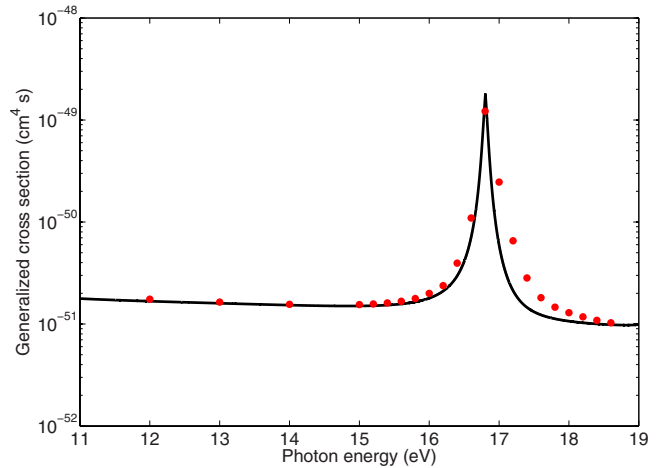

FIG. 3. (Color online) Generalized cross section for two-photon ionization of Ne as function of photon energy. The filled circles represent the results obtained using the current TDRM approach. The solid line represents results obtained by McKenna and van der Hart using the RMF approach. (The RMF results were shifted by -0.315 eV.) The present results were obtained by using a laser pulse with a peak intensity of $I_0 = 10^{12}$ Wcm^{-2}.

generalized cross sections for Ne with cross sections obtained using the time-independent RMF method. We use the same atomic structure basis as described above. However, in order to obtain TDRM cross sections which are comparable to the RMF results, we irradiate Ne with a 100 cycle (30 fs) laser pulse and therefore extend the *R*-matrix external region to a radius $a_p = 1000$ a.u. We obtain the generalized cross section $\sigma^{(N)}$ in units of cm^{2N} s^{N-1} for *N*-photon ionization from the relation

$$\sigma^{(N)} = (8\pi\alpha)^N \left(\frac{3.5 \times 10^{16}}{I}\right)^N \omega^N \Gamma a_0^{2N} t_0^{N-1}, \qquad (51)$$

where I is the intensity in W cm^{-2}, ω is the laser frequency in a.u., α is the fine-structure constant, and a_0 here is the atomic unit of length and is not to be confused with the radius of the *R*-matrix inner region boundary. t_0 is the atomic unit of time. Γ here is the total ionization rate which is obtained using the TDRM method by investigating the increase in the norm of the external region wave function beyond a radial distance of $r = 80$ a.u. Figure 3 shows our results for the generalized two-photon cross section of Ne in a photon energy region from 11 to 19 eV compared to results obtained using the RMF method. Agreement between the two sets of results is excellent, typically within 5% of each other away from resonance. The poorer agreement for energies close to the resonance structure corresponding to the $2p^5 3s$ $^1P^o$ state is due to the finite bandwidth of our pulse which is not present for the infinitely long pulse described in the RMF approach. As a consequence, the RMF pulse can resolve the sharp structure, whereas we obtain a broader resonance peak due to the frequency width of our pulse. It should also be noted that the RMF results have been shifted by -0.315 eV to compare with the TDRM results. The reason for the resonance appearing at different energies for the two methods is due to the fact that a larger configuration-interaction basis

was used for the current TDRM calculations and therefore the atomic structure is better described in the current TDRM approach.

As a third means of verifying the capability of the TDRM method, we apply it to the study of electrons ejected from multielectron atoms irradiated by a sequence of extreme ultra-violet (XUV) attosecond pulses. The momentum distributions of electrons ejected from Ne by light fields combining optical radiation and sequences of ultrashort light pulses are currently receiving considerable interest [26,27]. The experimental results show noticeable interference structures arising from the wave packets generated by the different ultrashort pulses. The experiments compared very well with theoretical results obtained using the strong-field approximation and semiclassical model calculations. In a recent report, we obtained momentum distributions for electrons ejected from Ne by a sequence of two ultrashort pulses in the presence of a 390 nm laser field using our recently developed RMI approach [19]. The results obtained using the RMI approach compared very well with a semiclassical model calculation. Due to the multielectron nature of the RMI approach, we were able to obtain momentum distributions for both emissions of a $2p$ electron and the emission of a $2s$ electron. Also, since the RMI approach is dedicated to treating complex atoms, a single calculation describes the emission of $2p$ electrons with both $|m| = 1$ and $m = 0$, which is not the case for SAE approaches.

In this paper, we apply our current TDRM method in order to obtain momentum distributions of electrons ejected from Ne by a sequence of two ultrashort pulses in the presence of a 780 nm laser field. Such a calculation is now made possible due to the fact that in the current TDRM method we can limit the computationally demanding calculation of the interelectronic and exchange effects between all the electrons in Ne to an *R*-matrix inner region and deal with an effective one-electron problem in the *R*-matrix outer region as dis-
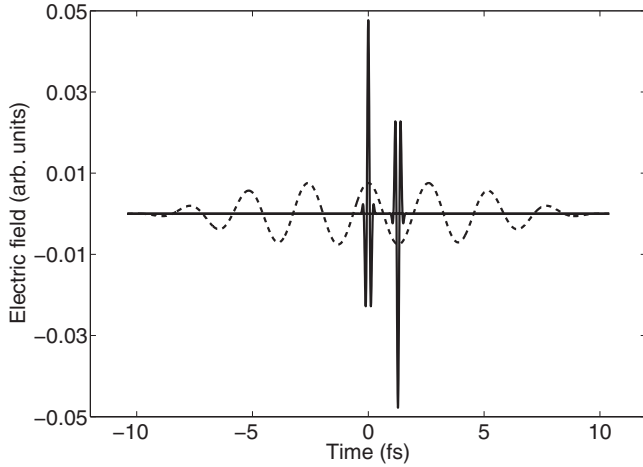
FIG. 4. Schematic of the electric field used in the present calculations. The dashed line shows the 780 nm laser pulse and the solid line shows the two ultrashort pulses.
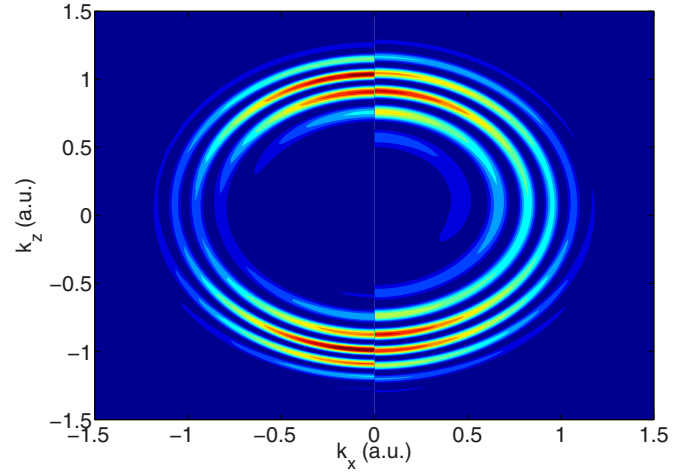

FIG. 5. (Color online) Momentum distributions $|k\phi(k)|^2$ in the $k_x k_z$ plane for the ejection of a $2p$ electron from Ne irradiated by 780 nm laser light and a sequence of two ultrashort pulses with delays as shown in Fig. 4. The distribution obtained using the TDRM approach is shown on the right half, while that obtained from the model is shown on the left half. The distributions are shown using a linear scale.

cussed in Secs. I and II. This division of the laser-atom interaction into a complex inner region problem and a simple outer region problem as seen in Fig. 1 is not present in the RMI approach which places a much greater computational demand on such box-based methods and therefore limits such approaches to much smaller problems.

The light field in the present calculations consists of a superposition of two fields, linearly polarized in the z direction: a short 780 nm laser pulse and two ultrashort light pulses. The 780 nm laser field has a three-cycle $\sin^2$ turn on of the electric field, two cycles at constant peak amplitude, followed by a three-cycle $\sin^2$ turn off. The ultrashort light pulses are made up a combination of the 17th, 19th, 21st and 23rd harmonics of the 780 nm radiation and a Gaussian time envelope. The first ultrashort pulse occurs at an extremum of the electric field for the 780 nm pulse and the second one occurs half a 780 nm cycle later. The field in the second ultrashort pulse has the opposite sign to the field in the first ultrashort pulse. A schematic of the light field is given in Fig. 4. The peak intensity of the 780 nm laser field was chosen to be 2.0×10^{12} W/cm^2 in order to suppress any multiphoton ionization due to this field. The peak of the ultrashort light pulse corresponds to an intensity of 5.0×10^{12} W/cm^2.

For the present calculations we use the same inner region basis as for the two-photon calculations described above. However, for these calculations the description of Ne includes all $1s^2 2s^2 2p^5 \varepsilon l$ channels up to L_{max}=9. Also, due to the long propagation time needed for wave packets moving in the presence of the 780 nm laser field, a large outer region radius of a_p=4000 a.u is required in order to prevent reflections of the wave function from the outer region boundary. The ability to propagate the R matrix and T vector out to such a large radial distance also greatly improves the momentum resolution, needed to observe interferences between the wave packets.

As discussed in Ref. [19], the basis set used in the inner region consists of multielectron wave functions, whereas the observable of interest is the momentum of a single outgoing electron. We therefore need to decouple the outer-electron

wave function from the full multielectron wave function and follow the same procedure as in Ref. [19]. Once we have obtained the channel functions, we need to decouple the spin and angular momentum of the continuum electron wave function from the Ne$^+$ target state. This decoupling can be done using Clebsch-Gordan coefficients. After we have obtained the wave function for the emitted electron, we transform it, for $r > 200$ a.u., into momentum representation under the assumption that the long-range Coulomb potential is negligible.

Figure 5 compares the ejected-electron momentum distributions obtained with the TDRM approach with those obtained using a simple model calculation. The model calculation is the same as that described in Ref. [19], in which it is assumed that the electrons are only emitted at the peak of an ultrashort pulse. Electrons emitted during the first ultrashort pulse then gain a phase difference with electrons emitted during the second ultrashort pulse of

$$\Delta\phi_1 = \left(\frac{k^2}{2} + E_{IP} \right) \Delta T, \qquad (52)$$

where k is the momentum of the outgoing electron, E_{IP} is the ionization potential of Ne, and ΔT is the time delay between the two pulses. The presence of the weak 780 nm laser field generates a second phase difference between the two pulses. Once a wave packet is generated, its center moves under the influence of the 780 nm laser field. At the time the second wave packet is generated, the center of the first wave packet is stationary with a displacement of $2E_0/\omega^2$ a.u. This displacement leads to an additional phase factor for the first wave packet of

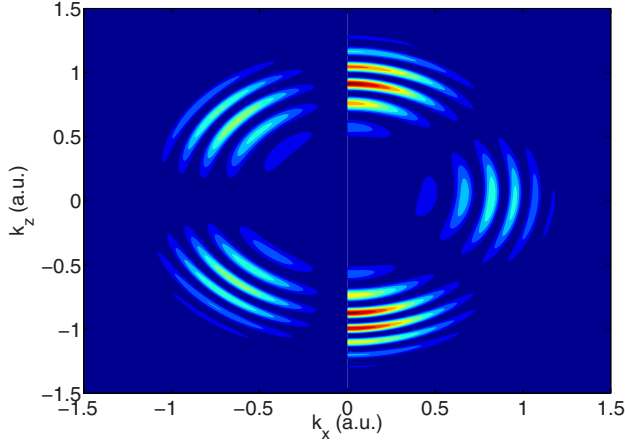$$\Delta\phi_2 = -2k_z \frac{E_0}{\omega^2}, \qquad (53)$$

FIG. 6. (Color online) Momentum distributions $|k\phi(k)|^2$ in the $k_x k_z$ plane for the ejection of a 2*p* electron from Ne irradiated by 780 nm laser light and a sequence of two ultrashort pulses with delays as shown in Fig. 4. Emission of $m=0$ is given on the right, while emission of $|m|=1$ is given on the left. The distributions are shown using a linear scale.

where k_z is the component of the momentum along the laser polarization axis and E_0 and ω are the field strength and frequency of the 780 nm radiation, respectively. The sign difference between the two pulses leads to an additional phase difference of π. Figure 5 shows that both momentum distributions are in good qualitative agreement with each other, verifying the capability of the present TDRM method to describe ultrafast dynamics of multielectron atoms.

As mentioned in Ref. [19], one of the key advantages of such a multielectron approach is that the emitted electron wave function separates naturally into its separate magnetic quantum number distributions. This is important when depletion of the initial state becomes appreciable since these emission processes compete with each other. Figure 6 shows the ejected-electron momentum distributions obtained for $m=0$ and $|m|=1$. These distributions are obtained from a single calculation, as opposed to SAE approaches where separate calculations are needed. The general behavior of these distributions is as expected from the properties of the Legendre polynomials.

The second main advantage of the TDRM approach is the capability to describe ionization leaving the residual ion in an excited state. Although we do not include a second target state in the present calculations, we have included the first excited state of Ne$^+$ in a separate study of ultrafast ionization processes and as a result have been able to study ultrafast ionization from the 2*s* shell in Ne [22].

IV. CONCLUSION

In conclusion, we have presented a detailed analysis of an *ab initio* 3D time-dependent *R*-matrix theory for ultrafast multielectron processes. This theory enables single ionization of atoms and atomic ions in intense ultrashort laser pulses to be accurately calculated. Our theory is completely *ab initio*, fully nonperturbative, and can be applied to an

arbitrary atomic system. We demonstrate the accuracy of the current approach by finding excellent agreement between Ne continuum wave functions obtained using the current method at the end of a 17 eV FEL pulse with those obtained using a separate time-dependent RMI method. We have compared generalized two-photon ionization cross sections for Ne obtained using the current method with results obtained using the time-independent RMF method and have found excellent agreement. We also verify the capability of the current approach by obtaining 2D momentum distributions of electrons ejected from Ne due to a sequence of two ultrashort pulses in the presence of a 780 nm laser pulse and finding very good qualitative agreement with a simple semiclassical model. It has also been shown in a separate study that ultrafast inner-shell processes in multielectron atoms can be described using the present method [22]. With the current scaling of experimental techniques to higher photon energies, shorter x-ray pulse durations and increasing stability [28], along with proposals for FEL-based attosecond sources [29], an accurate understanding of ultrafast inner-shell processes will become of increasing importance, and as a result the method presented here represents a timely and significant development for the realistic and accurate computation and understanding of such ultrafast multielectron dynamics.

APPENDIX: LONG-RANGE POTENTIALS

In this appendix we derive the explicit form of the long-range potential coupling the channels in Eq. (35) in the length gauge.

1. W_E term

This term is given by

$$W_E = \langle r_{N+1}^{-1} \bar{\Phi}_p^{\gamma}(r_{N+1}^{-1}) | \sum_{j=1}^{N} \frac{1}{|\mathbf{r}_{N+1} - \mathbf{r}_j|} - \frac{N}{r_{N+1}} | r_{N+1}^{-1} \bar{\Phi}_{p'}^{\gamma'}(r_{N+1}^{-1}) \rangle.$$

(A1)

We now expand

$$\sum_{j=1}^{N} \frac{1}{|\mathbf{r}_{N+1} - \mathbf{r}_j|} = \sum_{j=1}^{N} \sum_{\lambda=0}^{\infty} \frac{r_j^{\lambda}}{r_{N+1}^{\lambda+1}} P_{\lambda}(\cos \theta_{j,N+1}), \qquad \text{(A2)}$$

where $\cos \theta_{j,N+1} = \hat{\mathbf{r}}_j \cdot \hat{\mathbf{r}}_{N+1}$ and we remember that in the external region $r_j < r_{N+1}$ for $j = 1, \dots, N$. It follows that

$$W_E = \sum_{\lambda=1}^{\infty} \frac{a_{ii'}^{\lambda \gamma}}{r^{\lambda+1}} \delta_{\gamma \gamma'}, \qquad \text{(A3)}$$

where the coefficients $a_{ii'}^{\lambda\gamma}$ are defined by

$$a_{ii'}^{\lambda\gamma}\delta_{\gamma\gamma'} = \langle r_{N+1}^{-1}\bar{\Phi}_p^{\gamma}(r_{N+1}^{-1})|\sum_{j=1}^{N}r_j^{\lambda}P_{\lambda}(\cos\theta_{j,N+1})|r_{N+1}^{-1}\bar{\Phi}_{p'}^{\gamma'}(r_{N+1}^{-1})\rangle.$$
(A4)

These matrix elements are the same as those occurring in electron-atom (or ion) collisions in the absence of a laser field.

2. W_D term

This term is given by

$$W_D = \langle r_{N+1}^{-1}\bar{\Phi}_p^{\gamma}(r_{N+1}^{-1})|D_N|r_{N+1}^{-1}\bar{\Phi}_{p'}^{\gamma'}(r_{N+1}^{-1})\rangle.$$
(A5)

The channel functions can be expanded in the form

$$\bar{\Phi}_p^{\gamma}(\mathbf{X}_N;\hat{r}_{N+1}\sigma_{N+1}) = \sum_{M_{L_i}m_{l_i}}\sum_{M_{S_i}m_i}(L_iM_{L_i}l_im_{l_i}|LM_L)$$
$$\times\left(S_iM_{S_i}\frac{1}{2}m_i|SM_S\right)\Phi_i(\mathbf{X}_N)r_{N+1}^{-1}$$
$$\times Y_{l_im_i}(\theta_{N+1},\phi_{N+1})\chi_{(1/2)m_i}(\sigma_{N+1}),$$
(A6)

where the quantities $(L_iM_{L_i}l_im_{l_i}|LM_L)$ and $(S_iM_{S_i}\frac{1}{2}m_i|SM_S)$ are Clebsch-Gordan coefficients. Substituting Eq. (A6) into Eq. (A5) yields after some algebra

$$W_D = (-1)^{L_i+L_i'+1}(2L'+1)^{1/2}(10L'M_L|LM_L)W(1L_i'Ll_i,L_iL')$$
$$\times\langle\Phi_i\|D_N\|\Phi_{i'}\rangle\delta_{SS'}\delta_{M_SM_S'}\delta_{S_iS_i'}\delta_{M_{S_i}M_{S_i}'}\delta_{M_LM_L'}\delta_{l_il_i'}, \quad (A7)$$

where $W(1L_i'Ll_i,L_iL')$ are Racah coefficients. In writing these and later equations we have adopted the phase convention of Fano and Racah for the spherical harmonics.

3. W_P term

This term is given by

$$W_P = \langle r_{N+1}^{-1}\bar{\Phi}_p^{\gamma}|\mathbf{E}(t)\hat{\boldsymbol{\epsilon}}\cdot\mathbf{r}_{N+1}|r_{N+1}^{-1}\bar{\Phi}_{p'}^{\gamma'}\rangle.$$
(A8)

As before, we expand the channel functions using equation Eq. (A6). We also make use of the orthonormality relation satisfied by the target states,

$$\langle\Phi_i|\Phi_{i'}\rangle = \delta_{ii'}.$$
(A9)

Then, taking the z axis along the polarization vector $\hat{\boldsymbol{\epsilon}}\cdot\mathbf{r}$, so that

$$\hat{\boldsymbol{\epsilon}}\cdot\mathbf{r} = z = r\cos\theta,$$
(A10)

we have

$$\langle Y_{l+10}|\hat{\boldsymbol{\epsilon}}\cdot\mathbf{r}|Y_{l0}\rangle = -i\left(\frac{l+1}{[(2l+1)(2l+3)]^{1/2}}\right)r \quad (A11)$$

and

$$\langle Y_{l-10}|\hat{\boldsymbol{\epsilon}}\cdot\mathbf{r}|Y_{l0}\rangle = i\left(\frac{l}{[(2l-1)(2l+1)]^{1/2}}\right)r, \quad (A12)$$

where we have adopted the Fano-Racah phase convention for the spherical harmonics. After some algebra, Eq. (A8) reduces to

$$W_P = i\mathbf{E}(t)(-1)^{L+L'}[(2l_i'+1)(2L+1)]^{1/2}\frac{(LM_L10|L'M_L)}{(l_i010|l_i'0)}$$
$$\times W(1l_i'LL_i,l_iL')a(l_i')r\delta_{SS'}\delta_{M_SM_S'}\delta_{S_iS_i'}\delta_{M_{S_i}M_{S_i}'}\delta_{L_iL_i'}$$
$$\times\delta_{M_{L_i}M_{L_i}'}\delta_{\alpha_i\alpha_i'},$$
(A13)

where

$$a(l_i') = \begin{cases}\dfrac{l_i'}{[(2l_i'-1)(2l_i'+1)]^{1/2}} & l_i = l_i'-1 \\[4mm] -\dfrac{(l_i'+1)}{[(2l_i'+1)(2l_i'+3)]^{1/2}} & l_i = l_i'+1.\end{cases}$$

(A14)

[1] M. Hentschel *et al.*, Nature (London) **414**, 509 (2001).
[2] G. Sansone *et al.*, Science **314**, 443 (2006).
[3] M. Uiberacker *et al.*, Nature (London) **446**, 627 (2007).
[4] J. Mauritsson, P. Johnsson, E. Mansten, M. Swoboda, T. Ruchon, A. LHuillier, and K. J. Schafer, Phys. Rev. Lett. **100**, 073003 (2008).
[5] M. Drescher *et al.*, Nature (London) **419**, 803 (2002).
[6] E. Goulielmakis *et al.*, Science **305**, 1267 (2004).
[7] J. S. Parker, B. J. S. Doherty, K. J. Meharg, and K. T. Taylor, J. Phys. B **36**, L393 (2003).
[8] J. S. Parker, K. J. Meharg, G. A. Mckenna, and K. T. Taylor, J. Phys. B **40**, 1729 (2007).
[9] J. S. Parker, B. J. S. Doherty, K. T. Taylor, K. D. Schultz, C. I. Blaga, and L. F. DiMauro, Phys. Rev. Lett. **96**, 133001 (2006).
[10] P. G. Burke, P. Francken, and C. J. Joachain, J. Phys. B **24**, 761 (1991).
[11] P. G. Burke and K. A. Berrington, *Atomic and Molecular Processes: An R-Matrix Approach* (IOP, Bristol, 1993).
[12] L. Feng and H. W. van der Hart, J. Phys. B **36**, L1 (2003).
[13] H. W. van der Hart, B. J. S. Doherty, J. S. Parker, and K. T. Taylor, J. Phys. B **38**, L207 (2005).
[14] H. W. van der Hart, Phys. Rev. Lett. **95**, 153001 (2005).
[15] H. W. van der Hart, Phys. Rev. A **73**, 023417 (2006).
[16] M. Abu-samha and L. B. Madsen, J. Phys. B **41**, 151001 (2008).
[17] P. G. Burke and V. M. Burke, J. Phys. B **30**, L383 (1997).
[18] H. W. van der Hart, M. A. Lysaght, and P. G. Burke, Phys. Rev. A **76**, 043405 (2007).
[19] H. W. van der Hart, M. A. Lysaght, and P. G. Burke, Phys. Rev. A **77**, 065401 (2008).

[20] X. Guan, O. Zatsarinny, K. Bartschat, B. I. Schneider, J. Feist, and C. J. Noble, Phys. Rev. A **76**, 053411 (2007).

[21] X. Guan, C. J. Noble, O. Zatsarinny, K. Bartschat, and B. I. Schneider, Phys. Rev. A **78**, 053402 (2008).

[22] M. A. Lysaght, P. G. Burke, and H. W. van der Hart, Phys. Rev. Lett. **101**, 253001 (2008).

[23] J. H. Wilkinson, *The Algebraic Eigenvalue Problem* (Oxford University Press, Oxford, 1965).

[24] K. L. Baluja, P. G. Burke, and L. A. Morgan, Comput. Phys. Commun. **27**, 299 (1982).

[25] P. G. Burke and K. T. Taylor, J. Phys. B **8**, 2620 (1975).

[26] T. Remetter *et al.*, Nat. Phys. **2**, 323 (2006).

[27] K. Varju *et al.*, J. Phys. B **39**, 3983 (2006).

[28] G. De Ninno, E. Allaria, M. Coreno, F. Curbis, M. B. Danailov, E. Karantzoulis, A. Locatelli, O. Mentes, M. A. Nino, C. Spezzani, and M. Trovo, Phys. Rev. Lett. **101**, 053902 (2008).

[29] A. A. Zholents and G. Penn, Phys. Rev. ST Accel. Beams **8**, 050704 (2005).